creative commons
COMMONS DEED

저작자표시-비영리-변경금지 2.0 대한민국

이용자는 아래의 조건을 따르는 경우에 한하여 자유롭게

- 이 저작물을 복제, 배포, 전송, 전시, 공연 및 방송할 수 있습니다.

다음과 같은 조건을 따라야 합니다:

저작자표시. 귀하는 원저작자를 표시하여야 합니다.

비영리. 귀하는 이 저작물을 영리 목적으로 이용할 수 없습니다.

변경금지. 귀하는 이 저작물을 개작, 변형 또는 가공할 수 없습니다.

- 귀하는, 이 저작물의 재이용이나 배포의 경우, 이 저작물에 적용된 이용허락조건을 명확하게 나타내어야 합니다.
- 저작권자로부터 별도의 허가를 받으면 이러한 조건들은 적용되지 않습니다.

저작권법에 따른 이용자의 권리는 위의 내용에 의하여 영향을 받지 않습니다.

이것은 이용허락규약(Legal Code)을 이해하기 쉽게 요약한 것입니다.

Disclaimer

dCollection

Master's Thesis

Synthesis of Boron Nitride Nanotubes Using Atmospheric Pressure Thermal Plasma Jet

Graduate School

Jeju National University

Department of Nuclear and Energy Engineering

Minseok Kim

June 2020

제주대학교 중앙도서관
JEJU NATIONAL UNIVERSITY LIBRARY

대기압 열플라즈마 제트를 이용한 질화붕소나노튜브 합성

지도교수 최 수 석

김 민 석

이 논문을 에너지화학공학 석사학위 논문으로 제출함

2020년 06월

김민석의 에너지화학공학 석사학위 논문을 인준함

심사위원장 정 만 희 ㊞

위 원 최 수 석 ㊞

위 원 우 승 민 ㊞

제주대학교 대학원

2020년 06월

제주대학교 중앙도서관
JEJU NATIONAL UNIVERSITY LIBRARY

Synthesis of Boron Nitride Nanotubes Using Atmospheric Pressure Thermal Plasma Jet

Minseok Kim

(Supervised by Professor Sooseok Choi)

A thesis submitted in partial fulfillment of the requirement for the degree of

Master of Engineering

June 2020

This thesis has been examined and approved

Thesis Director — Department of Nuclear and Energy Engineering
Prof. Manhee Jeong — College of Engineering, Jeju National University

Thesis Committee Member — Department of Nuclear and Energy Engineering
Prof. Sooseok Choi — College of Engineering, Jeju National University

Thesis Committee Member — Department of Nuclear and Energy Engineering
Prof. Seungmin Woo — College of Engineering, Jeju National University

Date June 2020

Department of Nuclear and Energy Engineering

GRADUATE SCHOOL

JEJU NATIONAL UNIVERSITY

제주대학교 중앙도서관
JEJU NATIONAL UNIVERSITY LIBRARY

Acknowledgements

The work in this dissertation has been partially reprinted from previous published work in the journal, ***Journal of Nanoscience and Nanotechnology***, volume 19, page 6264–6270, October 2019. I am the primary author to this article, while Jeong-Hwan Oh, Tae-Hee Km, Yong Hee Lee, Seung-Hyun Hong, and Sooseok Choi are also contributors.

I also acknowledge previously published work has been partially reprinted from the journal, ***Chemical Engineering Journal***, volume 395, page 125148, September 2020. I am the primary author to this article, while Yong Hee Lee, Jeong-Hwan Oh, Byeong-Il Min, Tae-Hee Kim, and Sooseok Choi are also contributors.

I sincerely acknowledge financial support provided from the ***Hyundai Motor Chung Mong-Koo Foundation***, Republic of Korea.

제주대학교 중앙도서관
JEJU NATIONAL UNIVERSITY LIBRARY

The dissertation is dedicated to my family.

제주대학교 중앙도서관
JEJU NATIONAL UNIVERSITY LIBRARY

Abstract

While maintaining atmospheric pressure, highly crystalline and small-diameter boron nitride nanotubes (BNNTs) were synthesized using a triple DC thermal plasma jet with continuous injection of respective B and h-BN feedstock. Triple torch configuration not only generates larger high temperature regions than single torch but also allows feedstock to directly penetrate the core of the plasma flame, the hottest area in the reactor. The synthesis reaction with hydrogen molecules was analyzed with thermodynamic equilibrium analysis. Liberated nitrogen radicals formed in the strong electrical field of the triple DC torch actively reacted with the B and h-BN feedstock and H_2 gas, forming boron–nitrogen–hydrogen intermediates that eventually grow into BNNTs. Production rates of BNNTs in relation to power and gas consumption were 1.05 g/h·kW and 0.92 g/h·slpm, respectively, resulting in the yields superior to those reported to date. As a result, the high production rates for BNNTs approaching 22 g/h was attained through injection of B feedstock, suggesting their extendibility to real-world applications. These findings suggest the industrial-scale production of BNNTs with atmospheric DC thermal plasma jet.

Keywords: Atmospheric DC thermal plasma; Boron nitride nanotubes; Synthesis; Thermodynamic equilibrium analysis; Production rates

제주대학교 중앙도서관
JEJU NATIONAL UNIVERSITY LIBRARY

Table of Contents

제주대학교 중앙도서관
JEJU NATIONAL UNIVERSITY LIBRARY

List of Tables

제주대학교 중앙도서관
JEJU NATIONAL UNIVERSITY LIBRARY

List of Figures

제주대학교 중앙도서관
JEJU NATIONAL UNIVERSITY LIBRARY

제주대학교 중앙도서관
JEJU NATIONAL UNIVERSITY LIBRARY

Chapter 1. Introduction

1.1. Characteristics of Boron Nitride Nanotubes.

Theory on existence of Boron Nitride Nanotubes (BNNTs) was first proposed in 1994 based on the structural similarities between graphite and hexagonal boron nitride (h-BN), which suggested BNNTs could be as structurally stable phase as Carbon Nanotubes (CNTs) [1]. BNNTs have immediately stimulated great interest because they are electrically insulating with a much wider band gap of 5.5 eV [2] than CNTs that are either metallic or semiconducting depending on their diameter and chirality [3]. Subsequently, the demand for BNNTs began to surge as it has been figured out that BNNTs possessed various excellent characteristics. For example, the axial Young's modulus of BNNTs has been founded out to be 1.22 Tpa [4]. BNNTs have also exhibited not only significant resistance to oxidation up to 800 ℃ in air [5] but also possibility into biocompatible materials without limitations stemmed from cytotoxicity [6]. BNNTs even can be dyed to color. Comparable characteristics on BNNTs and CNTs are summarized in Table 1.1. These characteristics have made BNNTs highly attractive nanofillers for the improvement of nanocomposites: electrically insulating polymeric composites with high thermal conductivity [7], mechanically reinforced composites [8], piezoelectric nanogenerators [9], non-toxic biomaterials [10], filters for purification [11]. These assorted applicability has triggered great industrial demand for BNNT materials, which required large scaled synthesis of BNNTs. However, high-cost of such BNNT materials stemming from low-yield has severely hampered the scientific research and industrial applications of them.

제주대학교 중앙도서관
JEJU NATIONAL UNIVERSITY LIBRARY

Table 1.1. Comparable characteristics between BNNTs and CNTs.

	Boron Nitride Nanotubes (BNNTs)	Carbon Nanotubes (CNTs)
Electrical properties	Electrically insulating [2]	Metallic and semiconducting
Mechanical properties [Tpa] (Axial Young's modulus)	1.22 [4]	1.33
Axial thermal conductivity [W/m·K]	~3,000	~3,500
Resistance to oxidation [℃]	Stable up to 800 [5]	Stable up to 300 to 400
Thermal neutron absorption cross section [b[a]]	^{10}B: 3800, ^{11}B: 767, and N: 1.9	C: 0.0035
Biocompatibility	Non cytotoxic [6]	Cytotoxic
Piezoelectricity [C/m^2]	0.25~0.4	No dipole
Color	White	Black

[a] b, barn=10^{-24} cm^2.

제주대학교 중앙도서관
JEJU NATIONAL UNIVERSITY LIBRARY

1.2. Various Synthesis Methods for BNNTs

Anodic arc discharge was introduced to discover fullerene [12], whereby thermal electrons generated from arc channels provided high thermal energy sufficiently to evaporate the target materials on a local arc spot. This extreme thermal environment enabled the first synthesis of crystalline BNNTs in 1995 [13] because BNNT synthesis required huge thermal energy due to rapid recombination of N_2 molecules at high temperature (>7,000 K) and a strong triple bond of N_2 molecules(dissociation energy ($\Delta H°$) = 945 kJ/mol). Subsequently, various methods have applied for BNNT synthesis: arc discharge [13,14], laser vaporization [15,16], chemical vapor deposition [17,18], ball milling with annealing [19,20]. Through these works, it seems that BNNT synthesis per se become commonplace at laboratory-scale but remains difficult at pilot-scale. It means the amount and quality of the produced BNNTs were inferior to those achieved with CNTs. However, a noteworthy advance on BNNT synthesis was achieved using thermal plasma jet recently [21-25].

1.3. BNNT Synthesis Using Plasma

Plasma arc discharge has been continuously developed for synthesizing BNNTs since the first synthesis of them [13,14], but it was hard to control the vaporization rate of the anode or cathode rod located in the reactor as the target materials for BNNT synthesis. Therefore, the yield from the plasma arc discharge methods is too low to apply in industrial applications. Subsequently, an arc plasma jet [21] was suggested to control the evaporation rate of feedstock because it indirectly provides thermal energy to target materials through a high-enthalpy jet medium. However, continuous operation was impossible because the synthesis was conducted in a reactor with the target materials located inside the reactor. To solve this problem, an original feedstock feeding system was introduced to continuously inject powder-type feedstock into the reactor of the arc plasma jet [22]. This system significantly increased not only operation time but also a yield because the tungsten cathode and copper nozzle anode

제주대학교 중앙도서관
JEJU NATIONAL UNIVERSITY LIBRARY

have longer lifetime than that of the consumable electrodes used as feedstock in previous studies [21]. However, a crucial drawback was the purity of the synthesized BNNTs because metal catalysts such as Ni and Y were used. The metal catalysts were attached to the top of the produced BNNTs because those metals played role of seeds for the growth into the tube structure.

Recently, a pilot-scale production of BNNTs by independently feeding h-BN powders as feedstock was performed using RF induction thermal plasma at atmospheric pressure without metal catalysts. This method enabled continuous production at a high rate approaching 20 g/h [23]. Subsequently, a yield of approximately 35 g/h was reported via inductively coupled thermal plasma with reactor pressurized up to 10 atm [24]. Boron (B) powders as feedstock were continuously injected to the system. Although both studies produced highly crystalline, few-walled, and small-diameter BNNTs, it would be advantageous for commercialization if a process could yield an analogous quality of BNNTs via the injection of B powders under atmospheric pressure. Comparable experimental conditions regarding large-scale synthesis of BNNTs using thermal plasma jet are summarized in Table 1.2.

Here, an atmospheric pressure DC thermal plasma jet with continuous and direct injection of B and h-BN powders and N_2 gas is introduced for large-scale synthesis of BNNTs. A triple torch configuration is applied into the thermal plasma reactor to produce an enlarged high temperature area, which allows feedstock to penetrate the high enthalpy plasma flame easily [25]. These works stemmed from our previous experiments on synthesis of metal boride nanoparticles covered with h-BN layers as shown in Fig. 1.1 [26]. The possibility of the reaction of B and N_2 in the thermal plasma reactor was confirmed through the synthesized h-BN layers, which led BNNT synthesis using the thermal plasma reactor [26]. Consequently, based on the BNNT synthesis results, effects of hydrogen injection into the synthesis reactor was investigated chemically and physically. Furthermore, production rates of BNNTs among various methods to date were compared according to their input power and gas usage.

제주대학교 중앙도서관
JEJU NATIONAL UNIVERSITY LIBRARY

Table 1.2. Comparable experimental conditions for large-scale synthesis of BNNTs using thermal plasma jet.

	Kim et al [23].	Fathalizadeh et al [24].	Present work [25].
Feedstcok	h-BN	B	h-BN and B
Plasma source	RF[a]	RF	DC[b]
Chamber pressure [atm]	0.9	Pressurized up to 10	1
Plasma forming gas [slpm[c]]	Ar: 75 and N_2: 55	N_2: 50	Ar: 12 and N_2: 24
Reactant gas [slpm]	H_2: 20	-	H_2: 8
Power [kW]	60	40	21

[a] RF, Radio Frequency.

[b] DC, Direct Current.

[c] slpm, standard liter per minute.

제주대학교 중앙도서관
JEJU NATIONAL UNIVERSITY LIBRARY

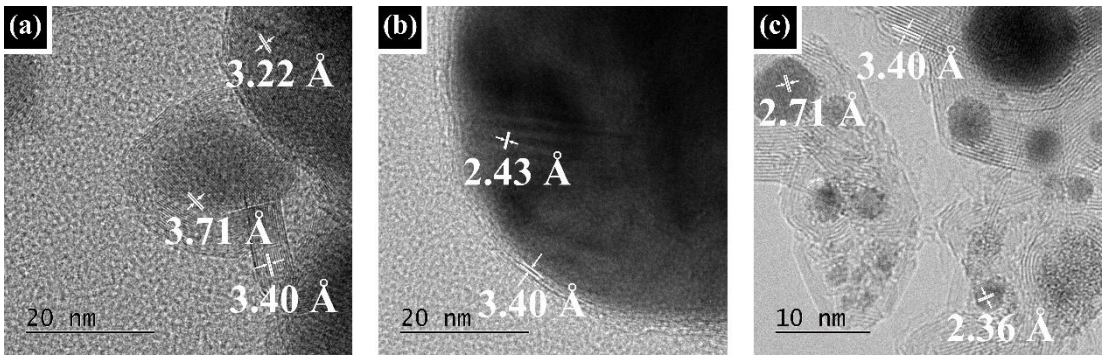

Figure 1.1. HR-TEM images for synthesized titanium (a), nickel (b), and tungsten (c) boride nanoparticles covered with h-BN layers. Lattice distance of 3.40 Å indicates that B feedstock and N_2 plasma forming gas reacted and formed h-BN phase in the thermal plasma reactor [26].

제주대학교 중앙도서관
JEJU NATIONAL UNIVERSITY LIBRARY

Chapter 2. Experimental Methods for BNNT Synthesis

2.1. Experimental Setup for BNNT Synthesis

The schematic diagram of the triple DC thermal plasma reactor for BNNT synthesis is presented in Fig. 2.1 (a). The system consists of three thermal plasma torches (Plasnix Co., Ltd., Republic of Korea), vertical reactors (R-1,2, and 3) and horizontal reactors (R-4, 5, 6, and 7), three DC power supplies up to 200 V, a cyclone filter, and a control box of cooling water and gases. The system maintained atmospheric pressure through a vacuum pump that exhausted continuous inflow of plasma forming gases and carrier gas for feedstock. The picture of the triple torch configuration (top image) and the operating moment (bottom image) when each plasma flame was formed with Ar gas is presented in Fig. 2.1 (b). The coalesced triple thermal plasma jet driven by Ar-N_2 plasma forming gases is shown in Fig. 2.1 (c), demonstrating that the length of the plasma flame reaches 30 cm without the confinement chamber.

The preliminary experiments for the torch operation were conducted according to the input power and gas usage and summarized in Table 2.1. A single set of conditions is applied to BNNT synthesis because the plasma flame was stable even after extended operation. h-BN (~1 μm, 98%, Sigma-Aldrich, Inc., USA) and B (~1 μm, 95%, Sigma-Aldrich, Inc., USA) powders were used as feedstock for BNNT synthesis, respectively. Each thermal plasma flame was produced by Ar (4 slpm) and N_2 (8 slpm). Thermally conductive H_2 and N_2 gas promote heat transfer for vaporization of the feedstock, which results in enlarged high temperature areas [27]. Especially, nitrogen molecule is essential for BNNT synthesis, thus Ar and N_2 mixed plasma forming gases were used to generate each thermal plasma flame. H_2 (8 slpm) gas was also injected into the reactor as reactant gas through the upper part of R-1 (Fig. 2.1 (a)). The input power of each torch was about 7 kW, total 21 kW, at a fixed current (100 A). The feedstock was injected with Ar carrier gas (5 slpm), and the feeding rate was about 0.5 g/min.

제주대학교 중앙도서관
JEJU NATIONAL UNIVERSITY LIBRARY

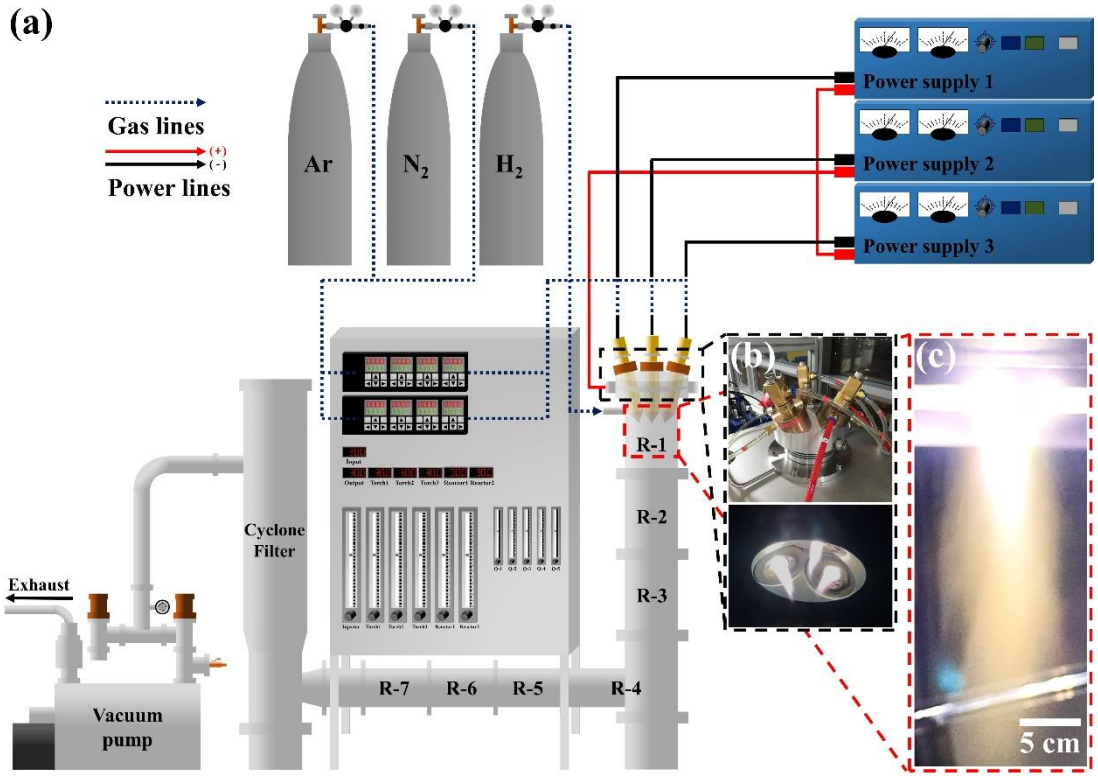

Figure 2.1. The schematic diagram (a) of the triple DC thermal plasma reactor. The picture (b) of the triple torch configuration. The merged moment (c) of the triple DC thermal plasma jet [25].

제주대학교 중앙도서관
JEJU NATIONAL UNIVERSITY LIBRARY

Table 2.1. Torch operation conditions according to the current and flow rate of plasma forming gases.

Current (A)	Ar (slpm)	N_2 (slpm)	Voltage (V)
80	5	7	64
		8	67
	4	6	60
		7	65
		8	68
		9	71
90	5	5	60
		6	64
		7	67
	4	6	65
		7	69
		8	72
100	5	5	60
		6	64
		7	67
	4	4	53
		6	64
		7	67
		8	70

제주대학교 중앙도서관
JEJU NATIONAL UNIVERSITY LIBRARY

The crystal structure of the synthesized BNNTs was analyzed by X-ray diffraction (XRD, Malvern Panalytical. Ltd., Empyrean, UK) with CuK_{α} radiation (λ = 1.5406 Å). The morphological properties and chemical composition of the synthesized BNNTs were analyzed via field emission scanning electron spectroscopy (FE-SEM, MIRA3, TESCAN, Czech) with energy dispersive spectroscopy (EDS, X-max, Oxford Instruments, UK) at 15 kV accelerating voltage. The synthesized BNNTs were coated by platinum using a sputter coater (Q150R S, Quarum, UK) to prevent from electron charging at a fixed current of 20 mA for 30 s. Detailed stratified appearance such as multi-walled structures of the produced BNNTs were observed through field emission transmission electron microscopy (FE-TEM, JEM-2100F, JEOL Ltd., Japan) at 200 kV accelerating voltage. Electron energy loss spectroscopy (EELS) analysis was performed at 200 kV accelerating voltage from a beam spot size 0.5 nm to confirm their chemical composition and bonding state of the synthesized BNNTs.

2.2. Thermodynamic Equilibrium Calculations

The process of BNNT synthesis was investigated theoretically by conducting thermodynamic equilibrium calculations using HSC Chemistry software (Ver. 9.1.1, Outotec Research Oy, Finland). The Gibbs free energy is defined by the following equation:

$$G = H - T \times S \tag{2.1}$$

Where the G is Gibbs free energy, H is enthalpy, T is temperature, and S is entropy. The enthalpy and entropy values are available in the databases. The change in Gibbs free energy indicates if the reaction is a spontaneous chemical reaction [28]. The thermodynamic reactions that form N_xH_y and B_xH_y gases were calculated with H_2 gas to explain why injection of H_2 gas is essential to the proposed BNNT synthesis reactor. Subsequently, the thermodynamic reactions that form boron nitride hydrogen (BNH and BNH_2) were calculated with the generated N_xH_y and B_xH_y molecules. In these chemical reactions, the temperature was ranged from 500 K to 10,000 K, and pressure was fixed at atmospheric pressure.

제주대학교 중앙도서관
JEJU NATIONAL UNIVERSITY LIBRARY

Chapter 3. Results and Discussion on BNNT Synthesis

3.1. BNNT Synthesis and Their Characterization

3.1.1. BNNT Synthesis Injecting h-BN Feedstock

XRD analysis for collected samples identify them as h-BN phase by their similarity on XRD pattern of the h-BN feedstock as shown in Fig. 3.1. The crystallinity of the synthesized BNNTs improved slightly as they far from the plasma flame, suggesting the correlation between residence time and the crystallinity of them. It means crystallinity for synthesized nano materials in the reactor can be improved by regulating residence time during synthesis process.

SEM images with macroscopic images of the BNNTs collected from the vertical and horizontal reactors are presented in Fig. 3.2 (a) and (b), respectively. A fabric-like material such as tangled threads was successfully formed in the triple DC thermal plasma reactor, which shows a thin cotton-like appearance at the macroscopic scale. Additionally, the length of the fabric-like material collected from the horizontal reactors was much longer than that from the vertical reactors, which suggested that the residence time of the feedstock in the reactor also influences on the length of the synthesized BNNTs. The vertical reactors are closer to the plasma flame than horizontal reactors, meaning that the grown BNNTs in vertical reactors had less time to grow into BNNT structure than that of horizontal reactors. This results suggest that residence time influences on crystallinity of the synthesized BNNTs as well as length of them.

EDS analysis provides the chemical composition of the BNNTs from the vertical and horizontal reactors as shown in Fig. 3.2 (c) and (d), respectively. The results demonstrate that the synthesized BNNTs from both reactors have almost identical ratios of boron and nitrogen. This suggests that boron and nitrogen are the component species of the fabric-like material although a carbon peak was also observed. It is regarded that the carbon peak came from the carbon tapes used for the SEM analysis.

제주대학교 중앙도서관
JEJU NATIONAL UNIVERSITY LIBRARY

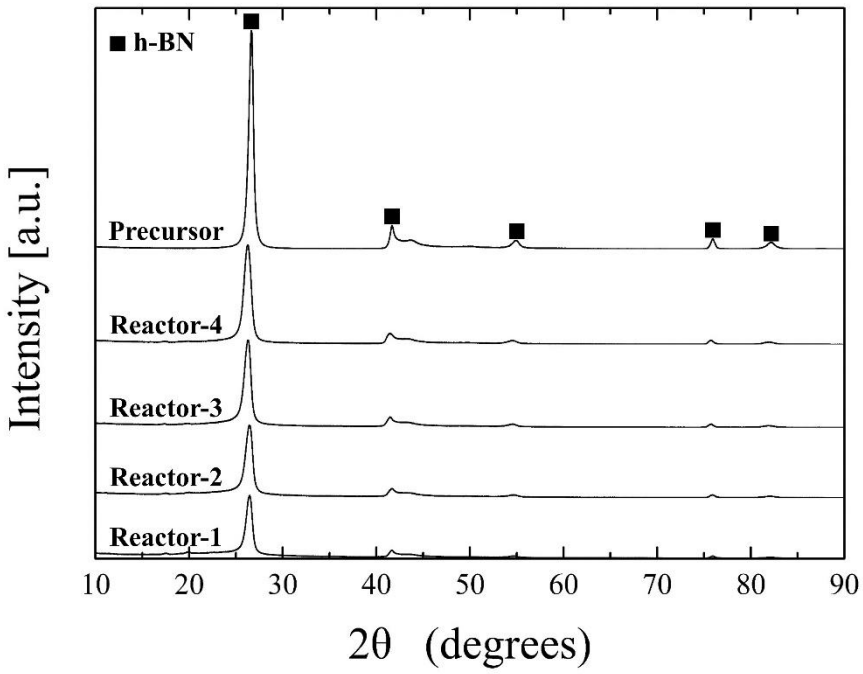

Figure 3.1. XRD patterns of h-BN feedstock and synthesized BNNTs at the vertical reactor from R-1 to R-4 [25].

제주대학교 중앙도서관
JEJU NATIONAL UNIVERSITY LIBRARY

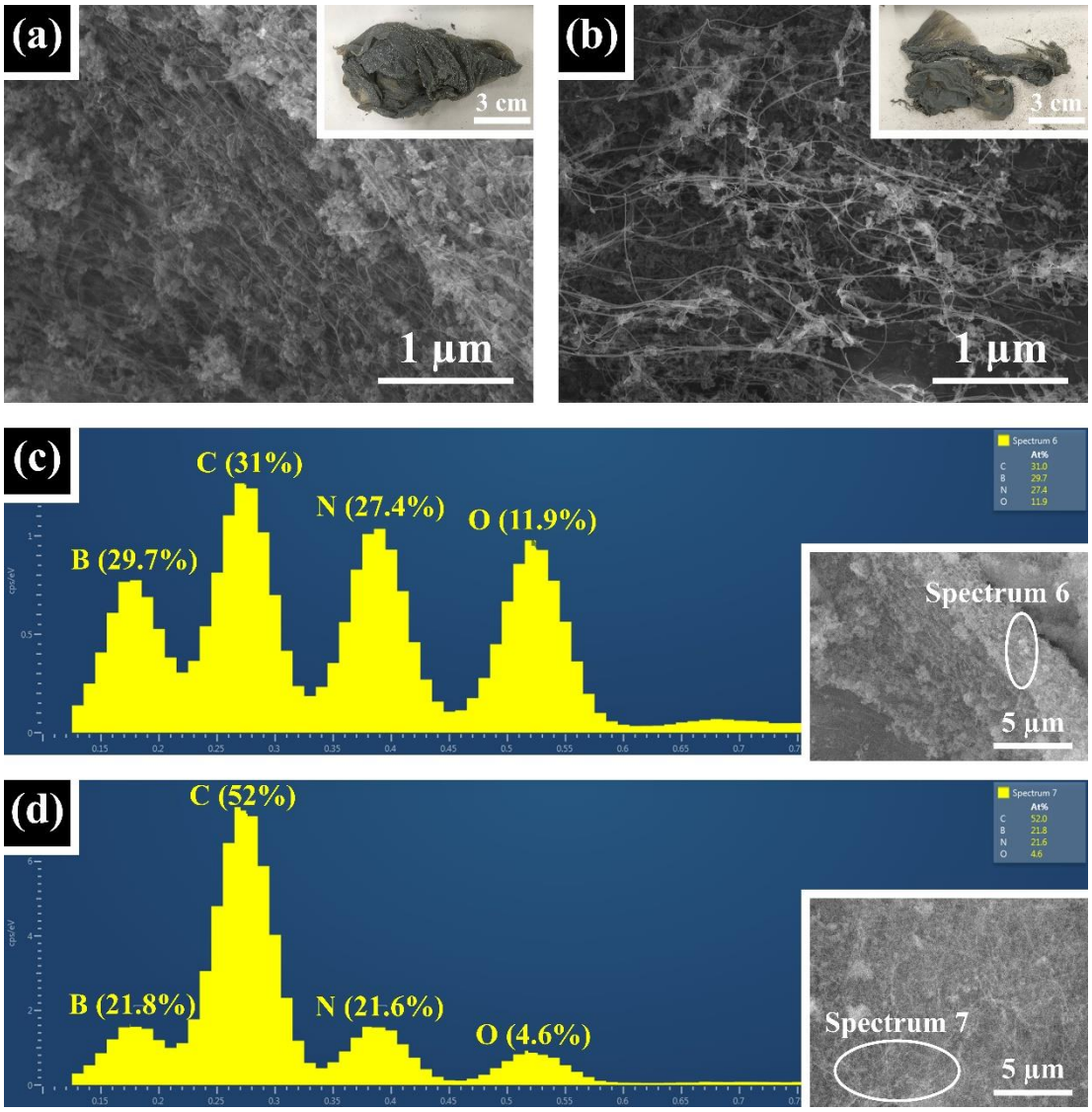

Figure 3.2. SEM and EDS analysis of the produced BNNTs according to the reactor. SEM and macroscopic images of the synthesized BNNTs from the vertical reactor (a) and horizontal reactor (b). EDS results for the synthesized BNNTs from the vertical reactor (c) and horizontal reactor (d) [25].

제주대학교 중앙도서관
JEJU NATIONAL UNIVERSITY LIBRARY

TEM analysis validated that the fabric-like material from the vertical and horizontal reactor has a tubular structure that are straight and parallel to the axis of the tube as shown in Fig. 3.3. Some single-walled BNNTs were observed, but the number of walls most frequently observed was 2 and 3, and majority of the BNNTs are three-walled. The D_{50} for the synthesized BNNTs is 7.05 nm (4.7 nm of Pt thickness by the sputter coater is considered). In addition, the multi-walled BNNTs have a highly crystalline structure with no evidence of the bamboo structures that result from relatively low temperature synthesis [19,20]. This highly crystalline structure was stemmed from a thermal plasma synthesis process that provides enough time for B-N-H intermediates to form crystal structure in the high temperature region [23-25]. Previous studies discussed the role of hydrogen on diameter distribution in the grown BNNTs but did not mention a role in the scale of synthesis [20]. By adding hydrogen gas to the synthesis of the BNNTs, the reaction presented in this study generates a high-yield rate of 12.6 g/h without metal catalysts [25].

3.1.2. BNNT Synthesis Injecting B Feedstock

The B feedstock also formed a spiderweb-like material as soon as injected in the reactor as presented in Fig. 3.4 (a). The accumulated white material conspicuously contrasted with the brown color of the B feedstock around the inlet of the feedstock, suggesting that the B feedstock reacted with the N_2 and H_2 gases immediately. The fabric-like material that formed around the torch inlets immediately filled the inside of the reactor during continuous operation. The very thin fabric-like material could have initially coated the inner wall of the reactor and then agglomerated into the tangled cotton-like material inside the reactor. Fig. 3.4 (b) and (c) show a wire-like structure that is considerably long up to tens of μm. Thus, the reactor chambers were filled with the cotton-like material. Unprecedented high-quality BNNTs were collected from a filter comprising three metal mesh rods as shown in Fig. 3.4 (d). The material suspended like spiderwebs between the three metal mesh rods appeared white to the naked eye and had a wire-like structure on the microscopic scale.

제주대학교 중앙도서관
JEJU NATIONAL UNIVERSITY LIBRARY

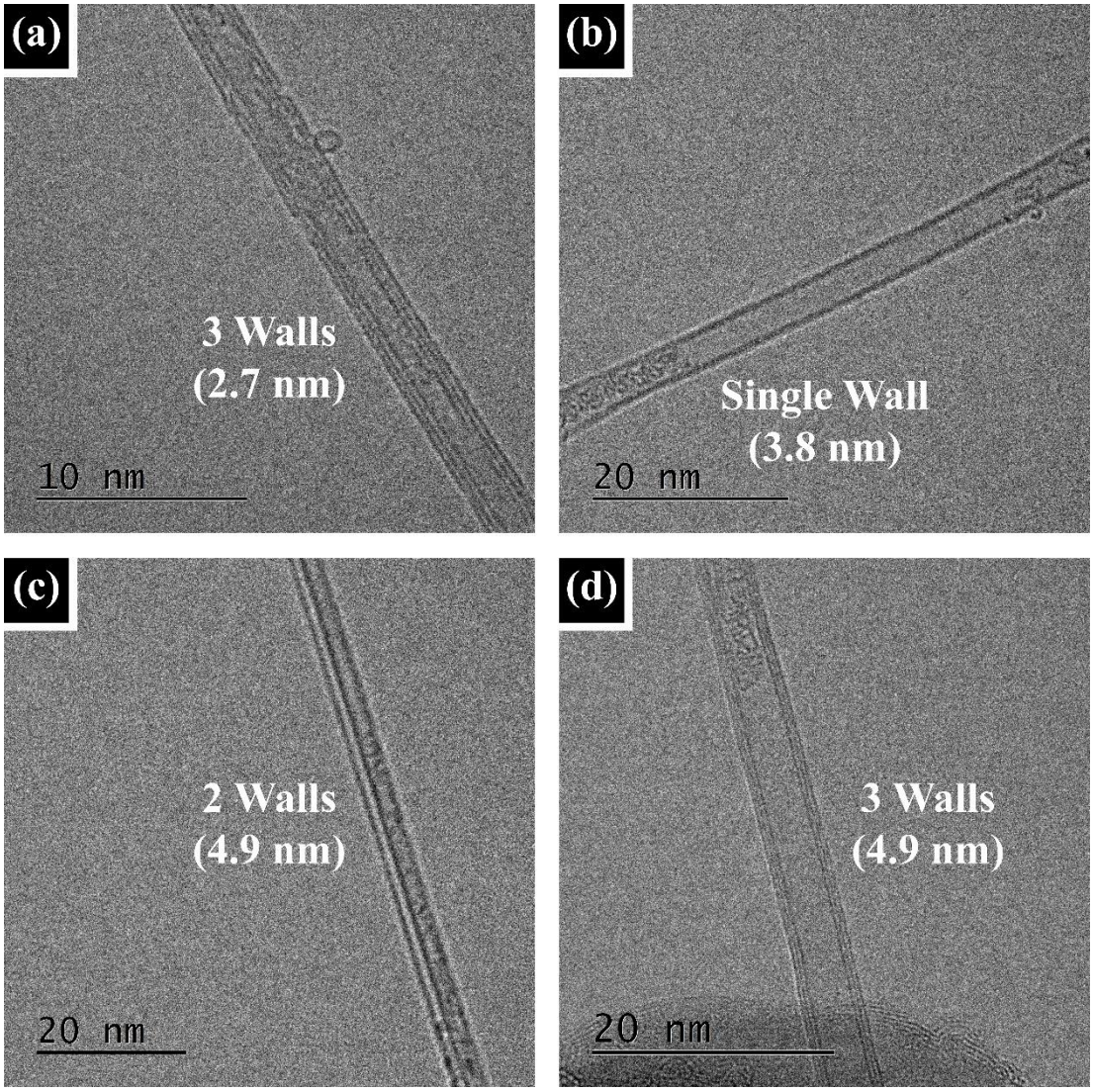

Figure 3.3. HR-TEM images of the synthesized BNNTs according to the reactor. (a) A three-walled BNNT whose diameter is approximately 2.7 nm and (b) a single-walled BNNT whose diameter is approximately 3.8 nm from the vertical reactors. (c) A double-walled BNNT whose diameter is approximately 4.9 nm and (d) a triple-walled BNNT whose diameter is approximately 4.9 nm from the horizontal reactor [25].

제주대학교 중앙도서관
JEJU NATIONAL UNIVERSITY LIBRARY

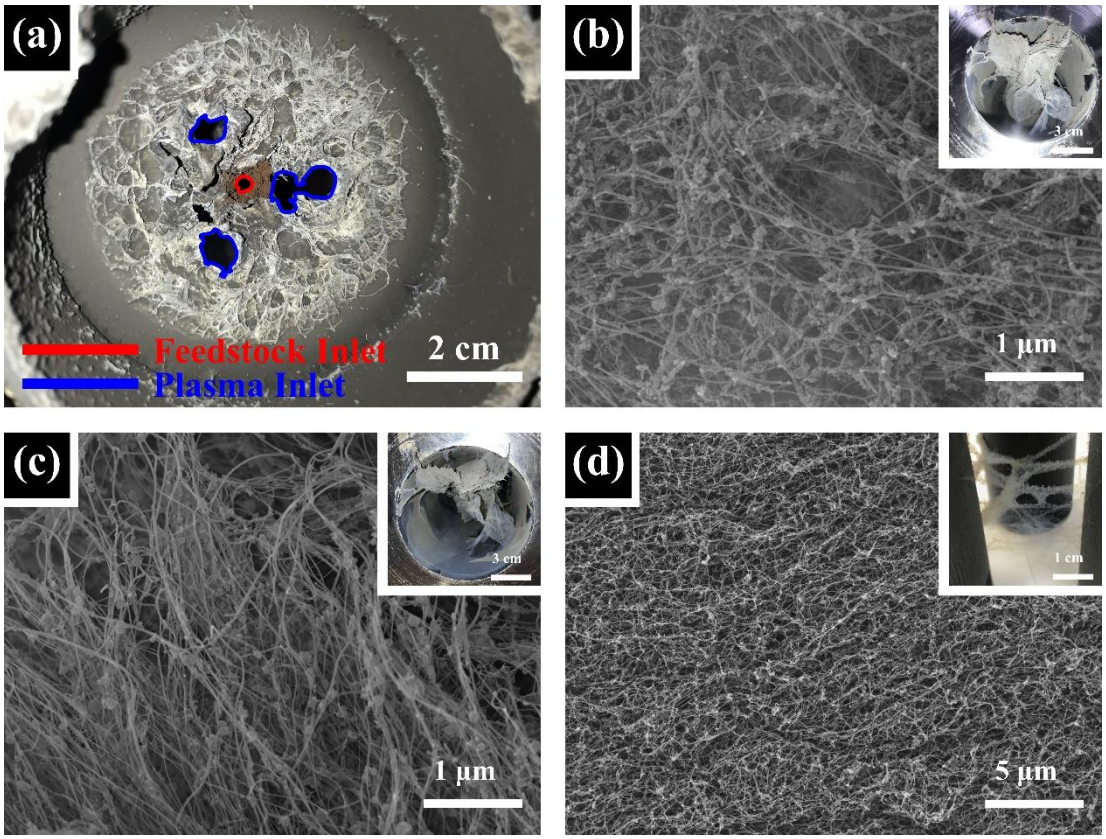

Figure 3.4. Macroscopic and SEM images of the material produced by the triple DC thermal plasma jet system. The initially formed material (a) piled up near the plasma and precursor inlet. Vertical reactor (b), horizontal reactor (c), and filter (d).

제주대학교 중앙도서관
JEJU NATIONAL UNIVERSITY LIBRARY

HR-TEM images show that the spiderweb-like material has a multi-tubular structure as shown in Fig. 3.5. Highly crystalline multi-walled structures between two and seven walls were observed. Owing to the deficiency of defects such as the bamboo structure and metal catalysts at the top of the BNNTs, the structural quality of the synthesized BNNTs was considerably higher than those obtained in previous studies [19,20,22]. Figure 3.6. presents an EELS profile for a tubular structure material produced by the triple DC thermal plasma jet system. K-edges arising from B (192 eV) and N (402 eV) were detected. These are composed of both π* and σ* peaks attributed to sp^2 hybridization. A weak carbon peak at 284 eV was also detected, which is regarded to originate from the carbon film on the TEM grid (holey carbon grid).

Diameter distribution of the synthesized BNNTs from the vertical and horizontal reactor and the cyclone filter is presented in Fig. 3.7. The diameter of the synthesized BNNTs increased with distance from the triple torch, resulting in D50 values of 10.63 nm, 14.4 nm, and 18.84 nm (a Pt thickness of 4.7 nm by the sputter coater was considered) for BNNTs obtained from the vertical reactor, horizontal reactor, and cyclone filter, respectively. This is consistent with previous experiments on the synthesis of nanoparticles that used our present system [25,26]. The nanotube structure and nanoparticles are regarded to become thicker with longer residence time in the reactors. Therefore, it is suggested that diameter of the BNNTs could be controlled by adjusting the residence time in the reactor.

제주대학교 중앙도서관
JEJU NATIONAL UNIVERSITY LIBRARY

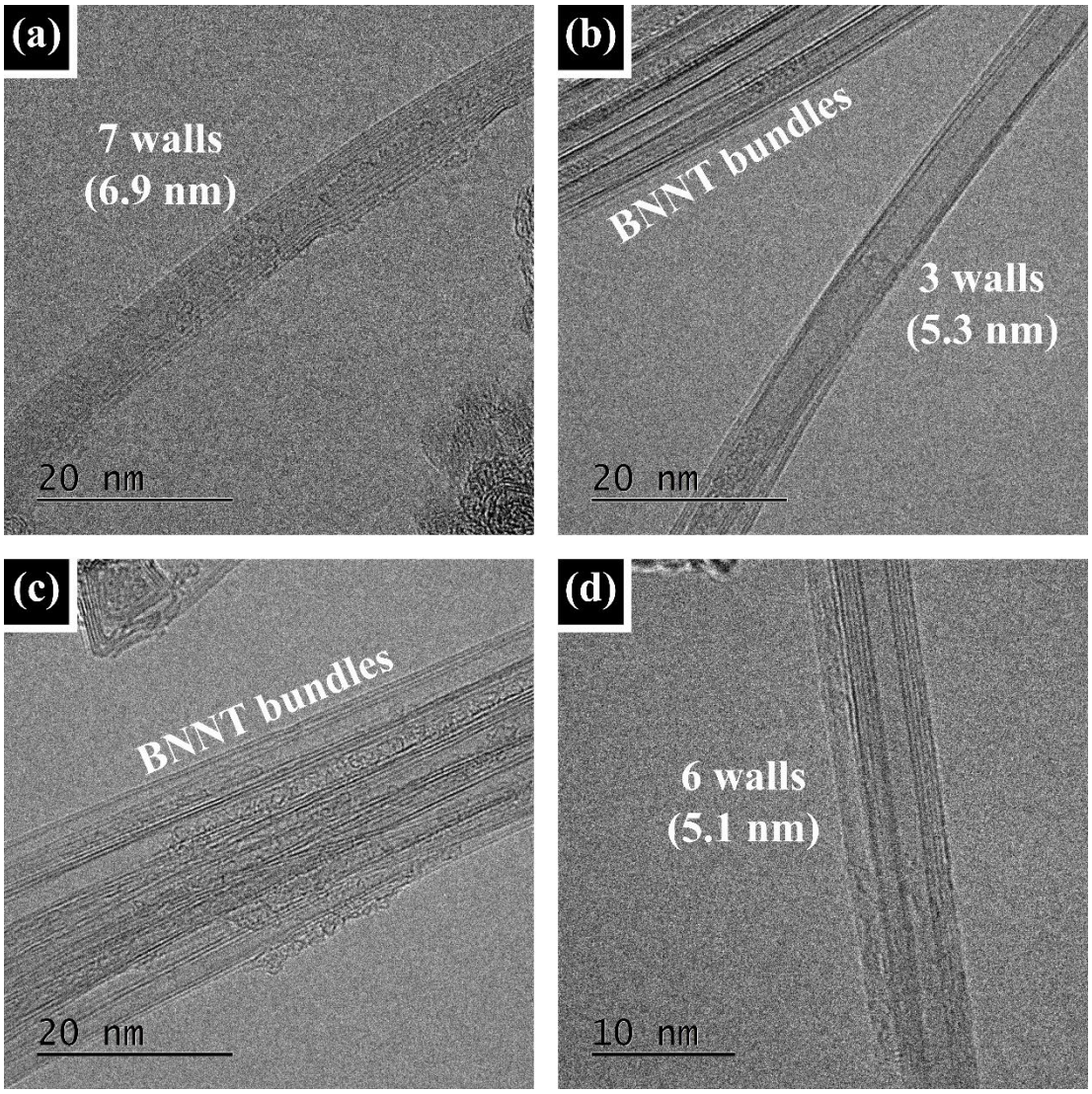

Figure 3.5. HR-TEM images of the BNNT material synthesized using the triple DC thermal plasma jet. A seven-walled BNNT (a), a three-walled BNNT with bundles, various-walled BNNT bundles (c), and a six-walled BNNT (d). The walls of each BNNT demonstrated a highly crystalline tube structure.

제주대학교 중앙도서관
JEJU NATIONAL UNIVERSITY LIBRARY

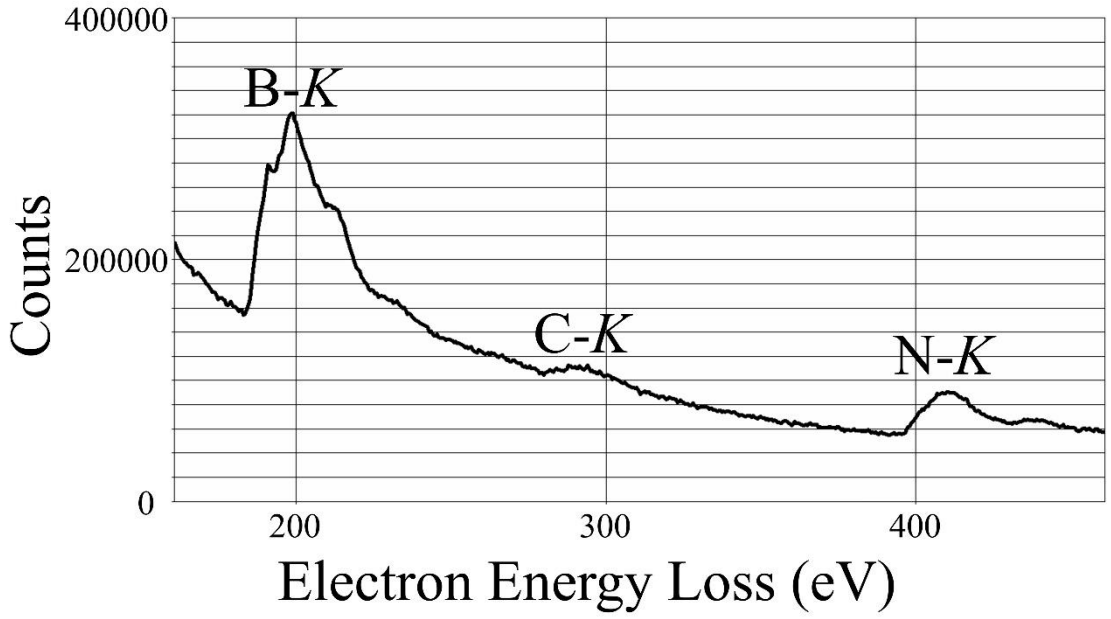

Figure 3.6. EELS profile for a BNNT with a diameter of ~5 nm.

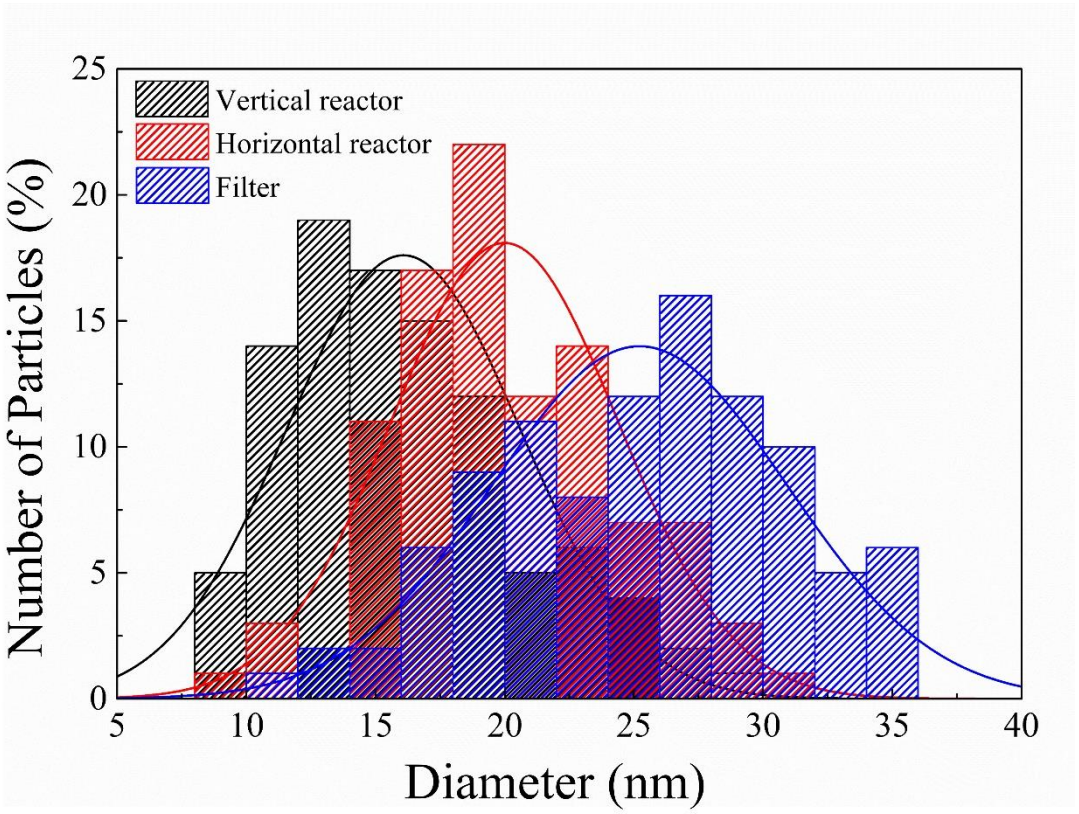

Figure 3.7. Diameter distribution of BNNTs according to the triple torch reactor regions. The distribution shows that the diameter of the BNNTs increased when approaching to filter.

제주대학교 중앙도서관
JEJU NATIONAL UNIVERSITY LIBRARY

3.2. Thermodynamic Equilibrium Analysis

Nitrogen is an essential source for BNNT growth. It decomposes and quickly recombines into N_2 in the high temperature (< 7,000 K) region. The direct nitration of B with N_2 dissociation into h-BN phase rarely occurs and is extremely slow due to the strong triple bond of nitrogen molecules. Figure 3.8 shows the change in the Gibbs free energy (ΔG) for the synthesis reaction that generates BN phase from B feedstock based on the boiling point of B (4,200 K). The blue line suggests that B in the gas state seldom reacts with N_2 gas because the blue line has positive values in the temperature regions above the boiling point of B. The green line has negative values from the boiling point of B to 5,255 K; the reaction is also hampered by the recombination of N gas, indicated by the orange dotted line located under the green line. However, the magenta line indicates the possibility of production BN gas using B and N species. The N_2 gas was injected between the cathode and anode of the triple torches and generated a thermal arc plasma jet. Therefore, the injected N_2 molecules were exposed to a strong electrical field and formed N radical ions by ionization. N^+ ions can be formed by both direct ionization of nitrogen species [29,30]:

$$N + e \rightarrow N^+ + 2e \text{ with a threshold energy of 14.5 eV} \quad (3.1)$$

$$N_2 + e \rightarrow N^+ + N + 2e \text{ with a threshold energy of 24.3 eV} \quad (3.2)$$

By continuously injecting N_2 gas into each plasma torch, the area around the triple torch contained abundant ionized N radical ions as shown in Fig. 3.9. These ionizations are highly dominant in the high electrical field between the cathode and anode of each torch so that it is regarded that N^+ ions participated in reaction to form N_xH_y molecules.

The red line in Fig. 3.10 (a) indicates the recombination between N radical ions and electrons. The blue, magenta, and green lines represent N_xH_y molecule formation from the reaction between N radical ions and hydrogen. At temperature below 5,072 K, the junction point of the red and green lines, the Gibbs free energy of the green line is lower than that of

제주대학교 중앙도서관
JEJU NATIONAL UNIVERSITY LIBRARY

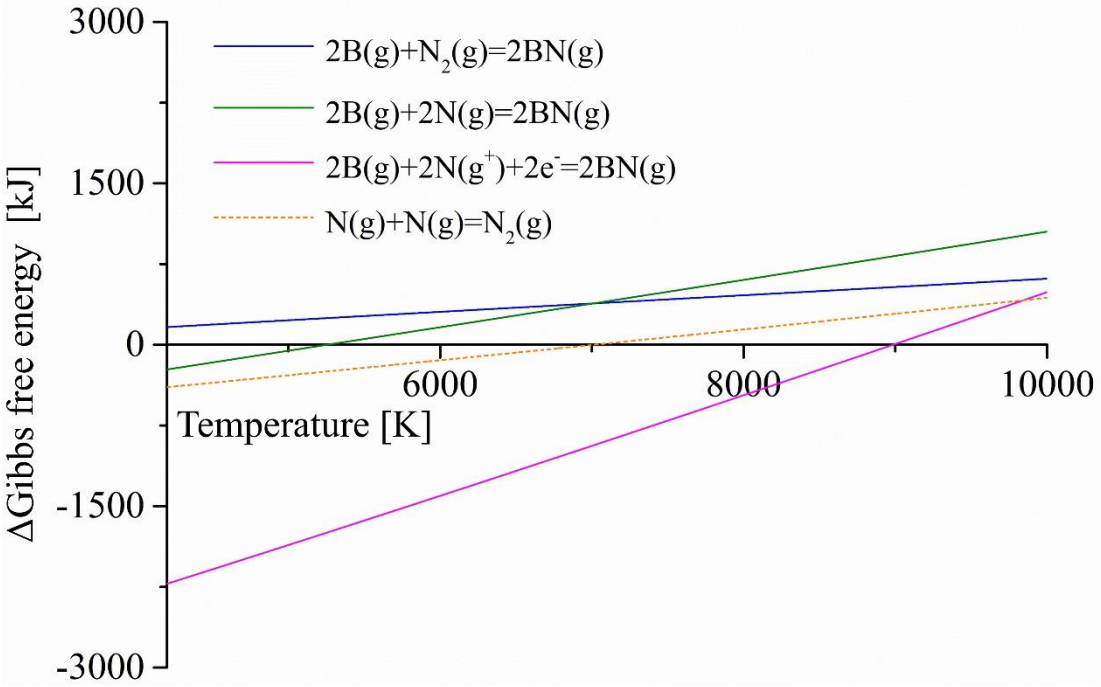

Figure 3.8. Thermodynamic equilibrium calculations from B feedstock to h-BN phase based on the boiling point of B (4,200 K).

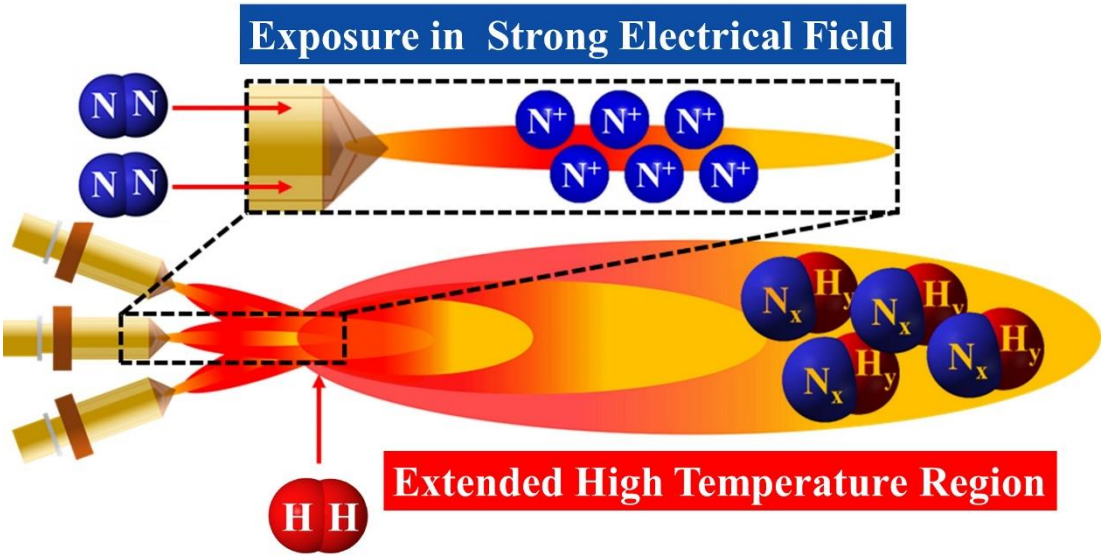

Figure 3.9. N radical ions formation through DC thermal plasma jet and reaction with H_2 reactant gas, which results in formation of N_xH_y molecules [25].

제주대학교 중앙도서관
JEJU NATIONAL UNIVERSITY LIBRARY

the red line, meaning that N_2H_2 formation is dominant from 3,743 K, the temperature at which hydrogen atoms recombine, to 5,072 K. These results show that the presence of hydrogen plays an essential role in the production of NH, NH_2, and N_2H_2 gases. The formed NH_2 and N_2H_2 molecules actively combine with BN gas, yielding BH_4 (blue and magenta lines) and BH_5 (green and orange lines) gases that are produced throughout the temperature range. This suggests that BN gas also plays an important role in the formation of BH_4 and BH_5 gases. BNH gas is formed by reactions between the formed BH_4 and BH_5 gases and the formed N_xH_y molecules as shown in Fig. 3.10 (c). In particular, BH_4 (blue and magenta lines) gas primarily combines with NH_2 and N_2H_2 gases, and BH_5 (green and orange lines) gas reacts preferentially with NH_2 and N_2H_2 gases to generate BNH under 10,000 K. BNH_2 gas formation reactions from the formed BH_4 and BH_5 gases and the formed NH, NH_2, and N_2H_2 gases are shown in Fig. 3.10 (d). BH_5 (orange line) shows the lowest Gibbs free energy in the Fig. 3.10 (d). These results suggest the reaction of N_2H_2 with BH_5 gas is crucial to the generation of the BNNTs because BNH and BNH_2 gas eventually produce BNNTs through a dehydrogenation reaction and formation of a boron droplet by nucleation [23]. Moreover, BNH are slightly more dominant than BNH_2 gas molecules. The chemical reaction pathway of BNNT synthesis from the plasma forming gas of N_2, the feedstock of B and h-BN, and the reactant gas of H_2 to BNH and BNH_2 is summarized in Fig. 3.11. These findings indicate that the reactions that form NH, NH_2, and N_2H_2 proceed primarily by the hydrogen-rich atmosphere; these reaction products are crucial for the formation of diverse BH gases and B-N-H intermediates (i.e., BNH and BNH2) that ultimately grow into BNNTs.

제주대학교 중앙도서관
JEJU NATIONAL UNIVERSITY LIBRARY

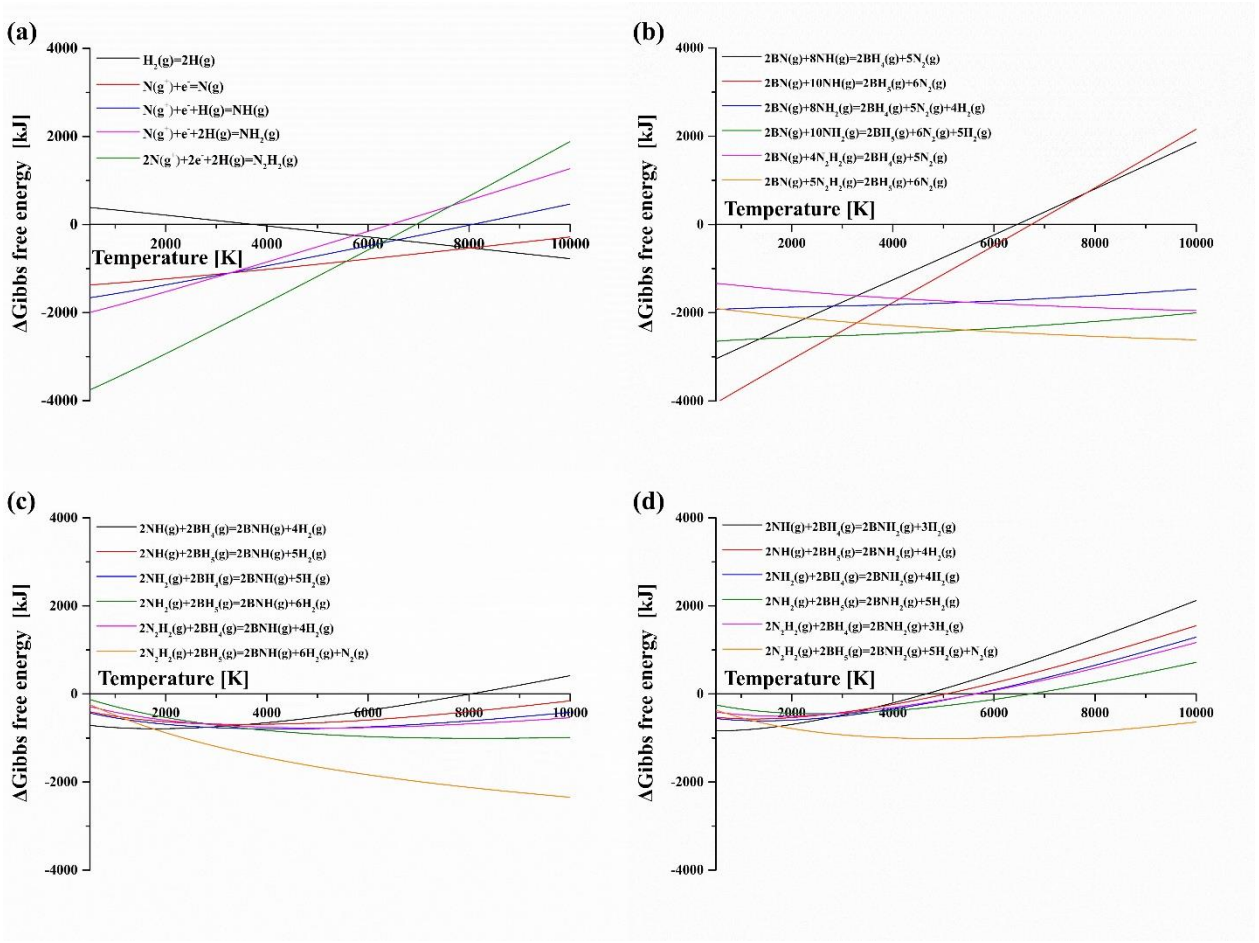

Figure 3.10. NH, NH_2, and N_2H_2 gas formations (a) from decomposed N radical ions. BH_4 and BH_5 gases formations (b) from BN gas and the formed NH, NH_2, and N_2H_2 gases. BNH (c) and BNH_2 (d) formation from the formed BH_4 and BH_5 gases and the formed NH, NH_2, and N_2H_2 gases [25].

제주대학교 중앙도서관
JEJU NATIONAL UNIVERSITY LIBRARY

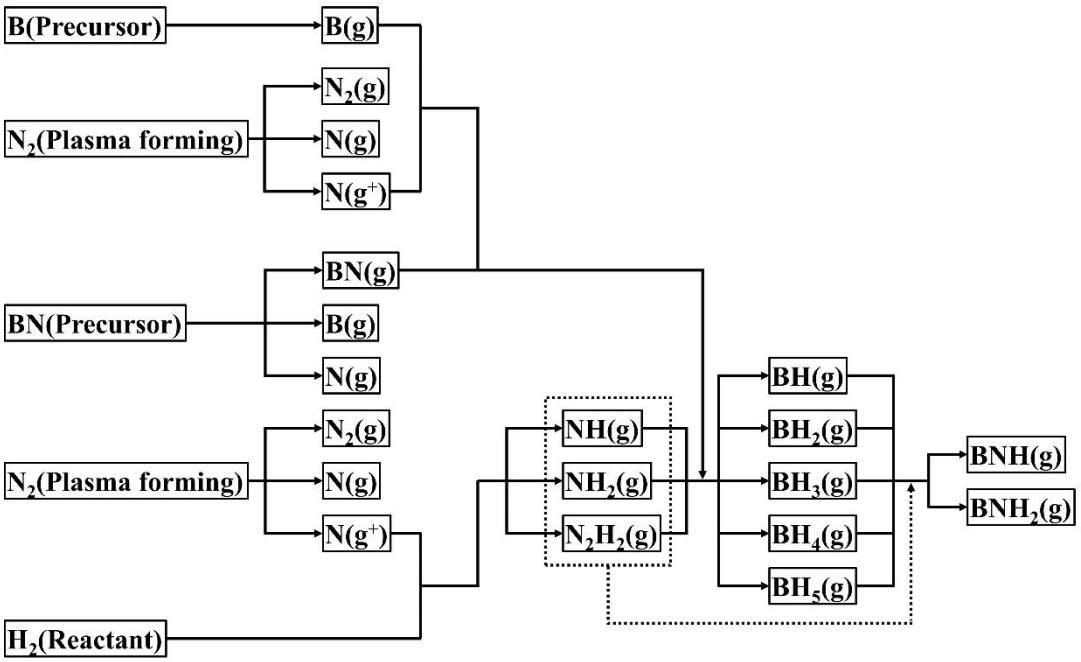

Figure 3.11. Proposed chemical reaction pathways for the BNNT synthesis with B and h-BN feedstock, N_2 plasma forming gas, and H_2 reactant gas [25].

제주대학교 중앙도서관
JEJU NATIONAL UNIVERSITY LIBRARY

3.3. Thermal Plasma Flow in the Reactor

Injection of hydrogen influences on BNNT synthesis physically as well as chemically. H_2 reactant gas was injected into the reactor in a direction perpendicular to the plasma jet at a flow rate of 8 slpm. Thermal conductivity of hydrogen gas is much higher than nitrogen gas in whole temperature range under 10,000 K [31,32]. The injection of hydrogen promotes that the heat in the reactor easily transferred to the surroundings such as walls of reactor. It also influences on viscosity of the thermal plasma jet flowing through the walls because viscosity of a fluid rises as temperature increases. Consequently, the thermal plasma flow in R-1 has higher viscosity near the walls than without hydrogen injection, which results in a strong adverse pressure gradient. The velocity of reverse flow near the walls was three times higher with the hydrogen injection than without it [25]. A large and strong vortex created by injecting hydrogen gas makes the feedstock such as B and h-BN recirculate inside the R-1, which provides enough time for them to chemically interact. It is regarded that such large vortex flow contributes mass production of BNNTs despite relatively low input power [23-25]. A comparison of production rate per input power and usage of nitrogen gas for the various BNNT synthesis methods is summarized in Table 3.1.

3.4. Gas-Phase Purification of BNNTs

Although efficient synthesis was achieved, it is difficult to say that all the synthesized materials had a nanotube structure. Unreacted feedstock that failed to grow into the nanotube structure forms nuclei in the reactor because B and BN vapors have high nucleation temperature. It is highly recommended to eliminate them through purification process because such impurities degrade the mechanical and chemical propertied of the BNNTs. Fig. 3.12 shows the change in the Gibbs free energy (ΔG) for gas-phase purification of BNNTs. It is regarded that fluorine gas among the halogens is the most effective to eliminate B and h-BN impurities as presented Fig. 3.12 (a) and (b). Based on the result regarding fluorine, gas-phase purification with fluorinated gases such as CF_4 and SF_6 was considered as shown in Fig. 3.12

제주대학교 중앙도서관
JEJU NATIONAL UNIVERSITY LIBRARY

(c). These fluorinated gases react with O_2 gas and impurities and formed BF_3 gas. Of course, by-products such as SO_2 and CO_2 gases are also generated but, these gases can be separately saved through low temperature distillation according to their boiling point. Furthermore, CF_4 and SF_6 gases are crucial threat of climate change. Their global warming potential is 6,500 and 23,900, respectively. Therefore, if this gas-phase purification process is applied to the BNNT synthesis reactor, it will not only improve the purity of the synthesized BNNTs but also contribute elimination of greenhouse gas that drives global climate change.

제주대학교 중앙도서관
JEJU NATIONAL UNIVERSITY LIBRARY

Table 3.1. Comparison of production rate per input power and usage of nitrogen gas for various BNNT synthesis methods [25].

Method	Feedstock	Input power [kW]	Production rate [g/h]	Production rates per power [g/h·kW]	Injection gas [slpm]	Production rates per nitrogen gas [g/h·slpm]
Laser ablation [15,16]	h-BN with B_2O_3	1–1.2	0.5–0.55	0.417–0.55	N_2: 4.8–7.2	0.07–0.11
	h-BN and B	1	0.12	0.12	-	-
Chemical vapor deposition [17]	Liquid $B_3H_6N_3$	-	0.2	-	-	-
	h-BN	-	0.016	-	Ar: 0.3 and NH_3: 0.2	0.08
RF thermal plasma [23,24]	h-BN	60	20	0.33	Ar: 75, N_2: 55, and H_2: 20	0.36
	B [24]	40	35	0.875	N_2: 50	0.7
DC thermal plasma [25]	h-BN	21	12.6	0.59	Ar: 12, N_2: 24, and H_2: 8	0.525
	B	21	22	1.05	Ar: 12, N_2: 24, and H_2: 8	0.92

제주대학교 중앙도서관
JEJU NATIONAL UNIVERSITY LIBRARY

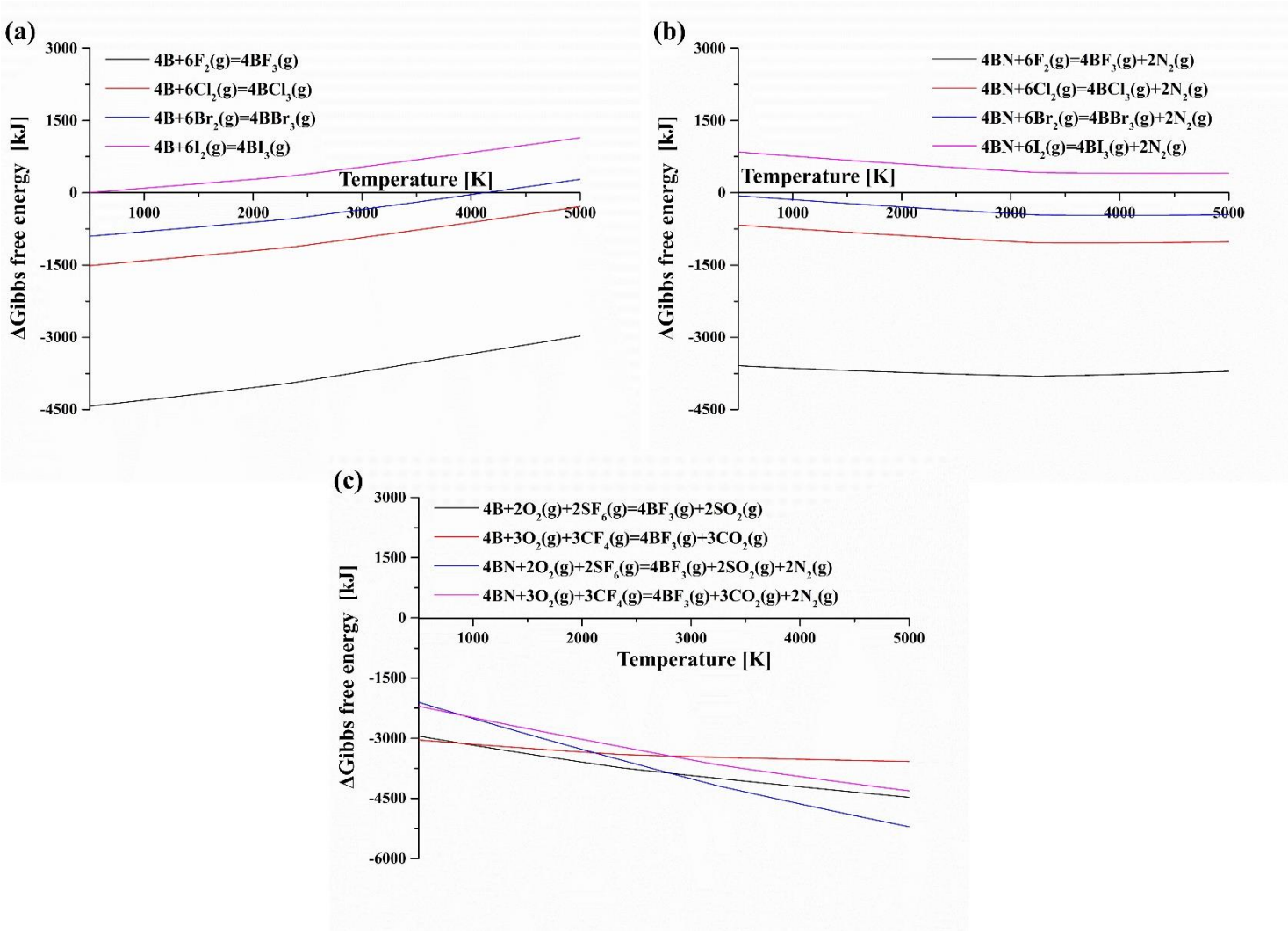

Figure 3.12. Thermodynamic equilibrium calculations with the halogens and fluorinated gases for gas-phase purification of BNNTs.

제주대학교 중앙도서관
JEJU NATIONAL UNIVERSITY LIBRARY

Chapter 4. Conclusion

Atmospheric pressure DC thermal plasma jet with continuous injection of respective B and h-BN feedstock was applied to BNNT synthesis reactor, which achieved high production rates of 22 g/h for highly crystalline and small-diameter BNNTs. Production rates per input power and gas usage is 1.05 g/h·kW and 0.92 g/h·slpm, respectively which is 20% and 31% improvement over the BNNT synthesis methods to date. It is regarded that a triple torch configuration contributed to the efficient production of BNNTs because it allowed the feedstock to penetrate to core of the coalesced plasma flame that possessed the highest thermal energy with the highest concentration of N radical ions. Furthermore, injection of hydrogen influenced on the efficient BNNT synthesis chemically and physically. Thermodynamic equilibrium analysis demonstrated that hydrogen molecules prevents the decomposed N radical ions from quickly recombining into N_2 and promotes the formation of NH, NH_2, and N_2H_2 gases. These gases generate various B_xH_y gases, which lead to the formation of B-N-H intermediates that eventually grow into BNNT structure through dehydrogenation reactions with early nucleation of B in the rapid quenching process. The hydrogen molecules also quickly transfer heat in the reactor due to their high thermal conductivity, resulting in large vortex area in the boron nucleation temperature region through strong adverse pressure gradient. The large vortex flow allows the B-N-H intermediates to recirculate in the reactive temperature region for an enough time to grow into the BNNTs.

제주대학교 중앙도서관
JEJU NATIONAL UNIVERSITY LIBRARY

References

[1] A. Rubio, J.L. Corkill, M.L. Cohen, Theory of graphitic boron nitride nanotubes, Phys. Rev. B. 49 (1994) 5081–5084.

[2] R. Saito, M. Fujita, G. Dresselhaus, M.S. Dresselhaus, Electronic structure of chiral graphene tubules, Appl. Phys. Lett. 60 (1992) 2204–2206.

[3] X. Blase, A. Rubio, S.G. Louie, M.L. Cohen, Stability and band gap constancy of boron nitride nanotubes, Europhys. Lett. 28 (1994) 335–340.

[4] N.G. Chopra, A. Zettl, Measurement of the elastic modulus of a multi wall boron nitride nanotube, Solid State Commun. 105 (1998) 297–300.

[5] Y. Chen, J. Zou, S.J. Campbell, G.L. Caer, Boron nitride nanotubes: Pronounced resistance to oxidation, Appl. Phys. Lett. 84 (2004) 2430–2432.

[6] X. Chen, P. Wu, M. Rousseas, D. Okawa, Z. Gartner, A. Zettl, C.R. Bertozzi, Boron nitride nanotubes are noncytotoxic and can be functionalized for interaction with proteins and cells, J. Am. Chem. Soc. 131 (2009) 890–891.

[7] C. Zhi, Y. Bando, T. Terao, C. Tang, H. Kuwahara, D. Golberg, Towards thermoconductive, electrically insulating polymeric composites with boron nitride nanotubes as fillers, Adv. Funct. Mater. 19 (2009) 1857–1862.

[8] C.Y. Zhi, Y. Bando, W.L. Wang, C.C. Tang, H. Kuwahara, D. Golberg, Mechanical and thermal properties of polymethyl methacrylate-BN nanotube composites, J. Nanomater. 2008 (2008) 1–5.

[9] S. Ye, C. Cheng, X. Chen, X. Chen, J. Shao, J. Zhang, H. Hu, H. Tian, X. Li, L. Ma, W. Jia, High-performance piezoelectric nanogenerator based on microstructured P(VDF-TrFE)/BNNTs composite for energy harvesting and radiation protection in space, Nano Energy. 60 (2019) 701–714.

[10] A. Merlo, V.R.S.S. Mokkapati, S. Pandit, I. Mijakovic, Boron nitride nanomaterials: biocompatibility and bio-applications, Biomater. Sci. 6 (2018) 2298–2311.

제주대학교 중앙도서관
JEJU NATIONAL UNIVERSITY LIBRARY

[11] T.A. Hilder, D. Gordon, S.H. Chung, Salt rejection and water transport through boron nitride nanotubes, Small. 5 (2009) 2183–2190.

[12] W. Krätschmer, L.D. Lamb, K. Fostiropoulos & D.R. Huffman, Solid C_{60}: a new form of carbon, Nature. 347 (1990) 354–358.

[13] N.G. Chopra, R.J. Luyken, K. Cherrey, V.H. Crespi, M.L. Cohen, S.G. Louie, A. Zettl, Boron Nitride Nanotubes, Science. 269 (1995) 966–967.

[14] Y.-W. Yeh, Y. Raitses, B.E. Koel & N. Yao, Stable synthesis of few-layered boron nitride nanotubes by anodic arc discharge, Sci. Rep. 7 (2017) 1–7.

[15] R. Arenal, O. Stephan, J.L. Cochon, A. Loiseau, Root-growth mechanism for single-walled boron nitride nanotubes in laser vaporization technique, J. Am. Chem. Soc. 129 (2007) 16183–16189.

[16] M.W. Smith, K.C. Jordan, C. Park, J. Kim, P.T. Lillehei, R. Crooks, J.S. Harrison, Very long single-and few-walled boron nitride nanotubes via the pressurized vapor/condenser method, Nanotechnology. 20 (2009) 505604.

[17] M.J. Kim, S. Chatterjee, S.M. Kim, E.A. Stach, M.G. Bradley, M.J. Pender, L.G. Sneddon, B. Maruyama, Double-walled boron nitride nanotubes grown by floating catalyst chemical vapor deposition, Nano Lett. 8 (2008) 3298–3302.

[18] Y. Huang, J. Lin, C. Tang, Y. Bando, C. Zhi, T. Zhai, B. Dierre, T. Sekiguchi, D. Golberg, Bulk synthesis, growth mechanism and properties of highly pure ultrafine boron nitride nanotubes with diameters of sub-10 nm, Nanotechnology. 22 (2011) 145602.

[19] Y. Chen, L.T. Chadderton, J.F. Gerald, J.S. Williams, A solid-state process for formation of boron nitride nanotubes, Appl. Phys. Lett. 74 (1999) 2960–2962.

[20] J. Yu, B.C.P. Li, J. Zou, Y. Chen, Influence of nitriding gases on the growth of boron nitride nanotubes, J. Mater. Sci. 42 (2007) 4025–4030.

[21] Y. Shimizu, Y. Moriyoshi, H. Tanaka, S. Komatsu, Boron nitride nanotubes, webs, and coexisting amorphous phase formed by the plasma jet method, Appl. Phys. Lett. 75 (1999)

제주대학교 중앙도서관
JEJU NATIONAL UNIVERSITY LIBRARY

929–931.

[22] C.M. Lee, S.I. Choi, S.S. Choi, S.H. Hong, Synthesis of boron nitride nanotubes by arc-jet plasma, Curr. Appl. Phys. 6 (2006) 166–170.

[23] K.S. Kim, C.T. Kingston, A. Hrdina, M.B. Jakubinek, J. Guan, M. Plunkett, B. Simard, Hydrogen-catalyzed, pilot-scale production of small-diameter boron nitride nanotubes and their macroscopic assemblies, ACS Nano. 8 (2014) 6211–6220.

[24] A. Fathalizadeh, T. Pham, W. Mickelson, A. Zettl, Scaled synthesis of boron nitride nanotubes, nanoribbons, and nanococoons using direct feedstock injection into an extended-pressure, inductively-coupled thermal plasma, Nano Lett. 14 (2014) 4881–4886.

[25] M. Kim, Y.H. Lee, J.-H. Oh, S.-H. Hong, B.-I. Min, T.-H. Kim, S. Choi, Synthesis of boron nitride nanotubes using triple DC thermal plasma reactor with hydrogen injection, Chem. Eng. J. 395 (2020) 125148.

[26] M. Kim, J.-H. Oh, T.-H. Kim, Y.H. Lee, S.-H. Hong, S. Choi, Synthesis of Metal Boride Nanoparticles Using Triple Thermal Plasma Jet System, J. Nanosci. Nanotechnol. 19 (2019) 6264–6270.

[27] T.-H. Kim, Y.H. Lee, M. Kim, J.-H. Oh, S. Choi, Thermal Flow Characteristics of the Triple Plasma Torch System for Nanoparticle Synthesis, IEEE Trans. Plasma Sci. 47 (2019) 3366–3373.

[28] H.B. Levine, Chemical equilibrium in complex mixtures, J. Chem. Phys. 36 (1962) 3049–3050.

[29] H.S. Uhm, Generation of various radicals in nitrogen plasma and their behavior in media, Phys. Plasmas. 22 (2015) 123506.

[30] S. Agarwal, B. Hoex, M.C.M. Van De Sanden, D. Maroudas, E.S. Aydil, Absolute densities of N and excited N_2 in a N_2 plasma, Appl. Phys. Lett. 83 (2003) 4918–4920.

[31] A.B. Murphy, C.J. Arundelli, Transport coefficients of argon, nitrogen, oxygen, argon-nitrogen, and argon-oxygen plasmas, Plasma Chem. Plasma Process. 14 (1994) 451–490.

제주대학교 중앙도서관
JEJU NATIONAL UNIVERSITY LIBRARY

[32] A.B. Murphy, Transport coefficients of hydrogen and argon-hydrogen plasmas, Plasma Chem. Plasma Process. 20 (2000) 279–297.

제주대학교 중앙도서관
JEJU NATIONAL UNIVERSITY LIBRARY

국문 초록

대기압 삼중 DC 열플라즈마를 사용하여 붕소 및 육방형 질화붕소 원료물질을 각각 연속적으로 주입하며 작은 직경 및 고 결정성을 갖는 질화붕소나노튜브를 합성하였다. 3중으로 구성된 DC 열플라즈마는 반응기 내에서 단일 토치보다 더 큰 고온 영역을 생성할 뿐만 아니라 원료 물질이 반응기의 가장 뜨거운 영역인 플라즈마 화염의 중심부로 직접 침투하는 것 또한 용이하게 한다. 반응성 기체로 수소를 주입함으로써 수소 주입의 영향을 열역학적 평형 계산을 통해 분석하였다. 플라즈마 발생 기체로서 DC 토치의 음극과 양극 사이로 주입되는 질소는 토치의 강한 전기장에 노출되어 해리됨으로써 질소 라디칼을 토치 영역 주변에서 형성한다. 본 라디칼은 반응 기체로 주입한 수소 및 붕소와 육방형 질화붕소 원료물질과 활발히 반응하여 붕소-질소-수소 중간체를 형성하며 최종적으로 질화붕소나노튜브로 성장하는 것으로 본 연구를 통해 제시되었다. 전력 및 가스 사용량과 관련한 질화붕소나노튜브의 생산량은 1.05 g/h・kW 및 0.92 g/h・slpm으로 현재까지 보고된 질화붕소나노튜브의 생산량들보다 우수하였으며, 결과적으로 붕소 원료 물질을 연속적인 주입을 통해 22 g/h에 달하는 질화붕소나노튜브의 높은 생산량이 달성되었다. 이러한 결과는 대기압 DC 열플라즈마 제트를 이용한 산업적 규모의 대용량 질화붕소나노튜브 합성을 제안한다.

중심어: 대기압 DC 열플라즈마; 질화붕소나노튜브; 합성; 열역학적 평형 분석; 생산량

제주대학교 중앙도서관
JEJU NATIONAL UNIVERSITY LIBRARY